J. Geophys. 43, 41 – 58, 1977

Journal of Geophysics

Finite-Difference Modelling for P-Pulse Propagation in Elastic Media with Arbitrary Polygonal Surface

A. Ilan

Department of Geophysics and Planetary Sciences, Tel-Aviv University, Tel Aviv, Israel

Abstract. The applicability of the finite-difference methods has been limited in most cases to simple geometric shapes. The problem of introducing boundary conditions into the scheme has usually restricted the models to structures in which the boundaries are parallel to the coordinates. Recently, several investigators have studied the effect of prominent topographic features on seismic signals. Most deal with SH waves. The behaviour of a P-SV pulse in media with prominent irregular surfaces is yet almost unknown. The difficulty of the last problem relative to the SH case lies in the vectorial form of the equation of motion and the more complicated boundary conditions.

In the present work a technique is proposed for simulating the P-SV wave propagation in a two-dimensional half-space with an arbitrary polygonlike topography. This technique has been applied to compute seismograms due to a P-pulse on surfaces of ridges and canyons. The incident pulse is amplified at the crest of mountains and at the upper corners of canyons. The magnitude of amplification is a function of the steepness of the topographic structure and can increase by 50% compared to a flat surface under the same conditions. The maximum attenuation computed at the bottom of a canyon was 25%. It can be concluded that the influence of prominent topographic features on the incident P-pulse is similar to that on incident SH waves, which was computed in previous investigations.

Key words: Finite-difference method – Wave propagation – Irregular surfaces.

1. Introduction

Field observations indicate that topography can have a significant effect on seismic signals. Boore (1972b) reported on very high accelerations of earth motions on top of mountains that sometimes exceed even the acceleration of

gravity, and can throw boulders out of their sockets. The highest ground acceleration that was so far recorded was 1.25 g. It occurred at Pacoima Dam site, California, as reported by Trifunac and Hudson (1971). Davis and West (1973) compared ground motions at the top and base of three different mountains. The peak motion at the crests were always larger than those at the bases, but the relation between respective amplitudes were different in every case.

This evidence indicates that structures which are prominent and convex cause amplification of the incident waves, but the ground motion at any particular site is influenced by numerous parameters and variables. The advantage of mathematical modelling is that the parameters can be changed at will, and one can therefore consider the effect of any geological and geometrical factor separately.

Some models were constructed for simulating wave-propagation in prominent topographic features. Boore (1972b, 1973) simulated SH wave-propagation in models of ridges and canyons. He approximated the topographic profiles by flat segments and 45 degrees steps. Trifunac (1973) and Wong and Trifunac (1974) solved analytically the problem of scattering of plane SH-waves by semi-cylindrical and semi-elliptical canyons. Wong and Jennings (1975) generalized the model, and included irregular canyons. Bouchon (1973) investigated the case of incident SH, P and SV waves on several types of topography, ranging from a ridge to a valley. He used the method of approximation developed by Aki and Larner (1970). Reimer et al. (1974) used a finite elements method to interpret the seismic response of Pacoima Dam in the San Fernando earthquake.

Most of the existing solutions deal with SH waves, but the main seismic energy is propagated by P-SV waves. The problem of P-SV wave propagation in an irregular structure is more difficult, because of the vectorial equation of motion and complicated boundary conditions.

The purpose of the present work was to develop a finite-difference technique for calculating the displacements caused by a P or SV pulse on elastic structures with an arbitrary polygonal surface. The method was applied to obtain theoretical seismograms on the surface of ridges and canyons. These seismograms were then used to detect regions of amplification or de-amplification comparable to a flat medium. Also to estimate the magnitude of amplification as a function of the slope of topographic features.

2. Model Assumptions

Let us consider a half-space with an arbitrary polygon-like free surface. The material is assumed to be perfectly elastic, isotropic, and homogeneous. α is the compressional, and β is the shear velocity. It was assumed that $\alpha = \sqrt{3}\beta$. A line source within the medium emits a compressional pulse. Let the y axis be along the line source and parallel to all the boundaries, thus the disturbance is in the x, z plane only. Let U and W be the horizontal and the vertical components of displacements, respectively. The wave propagation is governed by the following

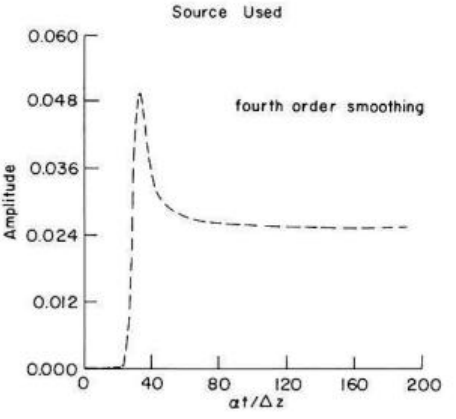

Fig. 1. The amplitude of the source function $S(r, t)$ plotted versus the dimensionless time $\alpha t/\Delta z$ at a distance of $20\Delta z$ from the source

equations of motion:

$$\frac{\partial^2 U(x,z,t)}{\partial t^2}=\alpha^2\frac{\partial^2 U(x,z,t)}{\partial x^2}+(\alpha^2-\beta^2)\frac{\partial^2 W(x,z,t)}{\partial x\,\partial z}+\beta^2\frac{\partial^2 U(x,z,t)}{\partial z^2}$$

$$\frac{\partial^2 W(x,z,t)}{\partial t^2}=\alpha^2\frac{\partial^2 W(x,z,t)}{\partial z^2}+(\alpha^2-\beta^2)\frac{\partial^2 U(x,z,t)}{\partial x\,\partial z}+\beta^2\frac{\partial^2 W(x,z,t)}{\partial x^2} \tag{1}$$

where t denotes the time.

Initially, at time $t=0$ the line source within the medium starts to emit a compressional pulse. The displacement due to the source at time t and at a distance $r=\sqrt{x^2+z^2}$ from the line source is given by:

$$S(r,t)=\frac{1}{\Delta^4}[G(r,t)-4G(r,t-\Delta)+6G(r,t-2\Delta)-4G(r,t-3\Delta)+G(r,t-4\Delta)] \tag{2}$$

where

$$G(r,t)=\frac{ar^3}{96\alpha^4}\left[\sqrt{\frac{t^2\alpha^2}{r^2}-1}\left(2\frac{t^3\alpha^3}{r^3}+13\frac{t\alpha}{r}\right)-3\left(4\frac{t^2\alpha^2}{r^2}+1\right)\log\left(\sqrt{\frac{t^2\alpha^2}{r^2}-1}+\frac{t\alpha}{r}\right)\right]H\left(\frac{t\alpha}{r}-1\right). \tag{3}$$

H is Heviside's unit step function and Δ is the parameter which determines the width of the pulse, a is constant. $S(r, t)$ satisfies the equations of motion (1). Its variation with time is illustrated in Figure 1. This source is suitable for finite difference schemes due to its high order of smoothness. For further details about the origin of the source functions and its qualities see Ilan and Loewenthal (1976).

The boundary conditions state – that all the components of stress are zero on the surface. The fulfillment of these boundary conditions on irregular surfaces is apparently the most difficult part of mathematical simulation of P-SV wave propagation. This difficulty limited the application of finite-difference methods

usually to simple models, where the surfaces are parallel to the coordinates. In the present paper the range of topography to which finite-differences can be applied will be enlarged gradually. The first step will be to develop a finite-difference scheme for obtuse wedges, because these are the basic elements of a polygon.

Finite-Difference Schemes for Obtuse Wedges

Alterman and Nathaniel (1975) solved the problem of P-pulse propagation in elastic wedges, using a special coordinate system parallel to the sides of the wedges. In this section the same problem is solved using cartesian coordinates, in order to enlarge the applicable geometry later to an arbitrary polygon.

Let the x axis be parallel to one side of the wedge and z pointed vertically upwards. The angle between the inclined free surface and the x axis is θ. A rectangular grid is superimposed on the wedge, and the mesh increments are chosen in such a manner that

$$\frac{\Delta z}{\Delta x}=\tan(\theta). \tag{4}$$

According to this choice the inclined surface passes through the diagonals of the mesh units, as illustrated in Figure 2. The horizontal and vertical displacements of the grid point (j, k) at time level p will be denoted $U^p_{j,k}$ and $W^p_{j,k}$ respectively.

By replacing the derivatives in Equations (1) by central finite differences the following formulae are obtained:

$$\begin{aligned}
U^{p+1}_{j,k} &= -U^{p-1}_{j,k}+2U^p_{j,k}+\alpha^2\left(\frac{\Delta t}{\Delta x}\right)^2(U^p_{j+1,k}-2U^p_{j,k}+U^p_{j-1,k})\\
&\quad+\beta^2\left(\frac{\Delta t}{\Delta z}\right)^2(U^p_{j,k+1}-2U^p_{j,k}+U^p_{j,k-1})\\
&\quad+\tfrac{1}{4}\frac{\Delta t^2}{\Delta x\,\Delta z}(\alpha^2-\beta^2)\\
&\quad\cdot(W^p_{j+1,k+1}-W^p_{j+1,k-1}-W^p_{j-1,k+1}+W^p_{j-1,k-1})\\
W^{p+1}_{j,k} &= -W^{p-1}_{j,k}+2W^p_{j,k}+\beta^2\left(\frac{\Delta t}{\Delta x}\right)^2(W^p_{j+1,k}-2W^p_{j,k}+W^p_{j-1,k})\\
&\quad+\alpha^2\left(\frac{\Delta t}{\Delta z}\right)^2(W^p_{j,k+1}-2W^p_{j,k}+W^p_{j,k-1})\\
&\quad+\tfrac{1}{4}\frac{\Delta t^2}{\Delta x\,\Delta z}(\alpha^2-\beta^2)\\
&\quad\cdot(U^p_{j+1,k+1}-U^p_{j+1,k-1}-U^p_{j-1,k+1}+U^p_{j-1,k-1}).
\end{aligned} \tag{5}$$

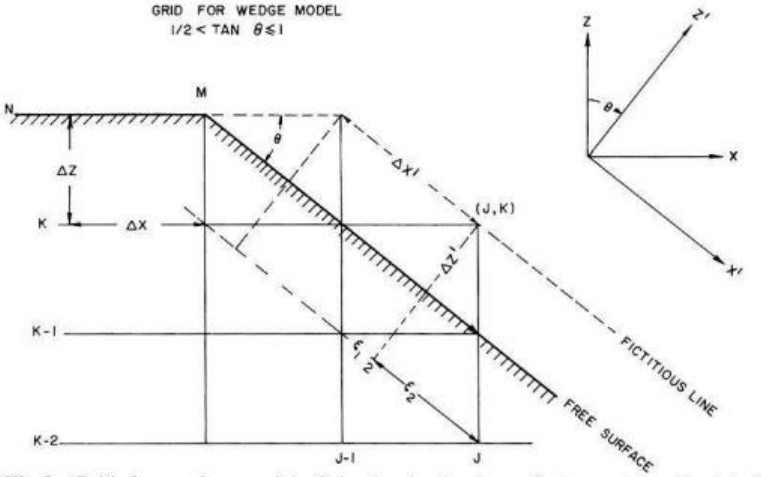

Fig. 2. Grid for wedge model, θ is the inclination of the wedge side, (z', x') are the suitable coordinates, and $(\Delta x', \Delta z')$ the local grid

On the horizontal free surface of the wedge the boundary conditions are:

$$\left.\begin{aligned} &\frac{\partial U(x,z,t)}{\partial z}+\frac{\partial W(x,z,t)}{\partial x}=0 \\ &(\alpha^2-2\beta^2)\frac{\partial U(x,z,t)}{\partial x}+\alpha^2\frac{\partial W(x,z,t)}{\partial z}=0 \end{aligned}\right\} z=n\Delta z,\ x\leqq m\Delta x. \tag{6}$$

The following approximations to Equations (6) were developed by Ilan et al. (1975) and improved by Ilan and Loewenthal (1976):

$$\begin{aligned} U_{j,k}^{p+1} &= -U_{j,k}^{p-1}+2\left[1-\beta^2\left(\frac{\Delta t}{\Delta z}\right)^2-\beta^2\left(\frac{\Delta t}{\Delta x}\right)^2(3-2\beta^2/\alpha^2)\right]U_{j,k}^{p} \\ &\quad +2\left(\frac{\Delta t}{\Delta z}\right)^2\beta^2 U_{j,k-1}^{p}+\beta^2\left(\frac{\Delta t}{\Delta x}\right)^2(3-2\beta^2/\alpha^2)(U_{j+1,k}^{p}+U_{j-1,k}^{p}) \\ &\quad -\beta^2\frac{\Delta t^2}{\Delta x\,\Delta z}(W_{j+1,k}^{p}-W_{j-1,k}^{p}) \\ W_{j,k}^{p+1} &= -W_{j,k}^{p-1}+2\left[1-\alpha^2\left(\frac{\Delta t}{\Delta z}\right)^2-\beta^2\left(\frac{\Delta t}{\Delta x}\right)^2\right]W_{j,k}^{p} \\ &\quad +2\alpha^2\left(\frac{\Delta t}{\Delta z}\right)^2 W_{j,k-1}^{p}+\beta^2\left(\frac{\Delta t}{\Delta x}\right)^2(W_{j+1,k}^{p}+W_{j-1,k}^{p}) \\ &\quad +0.5\frac{\Delta t^2}{\Delta x\,\Delta z}(3\beta^2-\alpha^2)(U_{j+1,k}^{p}-U_{j-1,k}^{p}) \\ &\quad -0.5\frac{\Delta t^2}{\Delta x\,\Delta z}(\beta^2-\alpha^2)(U_{j+1,k-1}^{p}-U_{j-1,k-1}^{p}) \end{aligned} \tag{7}$$

here (j, k) is a grid point on the horizontal free surface.

$z=n\Delta z, \quad x\leqq m\Delta x.$

$m\Delta x$ denotes the corner of the wedge.

This scheme is consistent with the boundary conditions (6) up to the second order of accuracy. It is stable even for very small β/α, and does not need the aid of fictitious points.

A special technique is needed only for the computation of the displacements on the inclined free surface. For that goal suitable cartesian coordinates are used, which are at an angle θ to the main system. Let (U, W) be the components of displacements in the rotated cartesian coordinates (x, z). An orthogonal transformation connects the components in the two different coordinate systems:

$$\begin{aligned} U' &= U\cos\theta - W\sin\theta \\ W' &= W\cos\theta + U\sin\theta. \end{aligned} \tag{8}$$

On the inclined free surface the boundary conditions are zero components of stress in the x' and z' direction. The mathematical expression of these conditions are the same as Equations (6) in the $(x'z')$ domain. A local grid is superimposed on the vicinity of the inclined surface. This grid includes a row of fictitious points, as shown in Figure 2. The dimensions of the intervals of the local grid are:

$$\begin{aligned} \Delta x' &= \frac{\Delta z}{\sin\theta} \\ \Delta z' &= \Delta z \cdot \cos\theta. \end{aligned} \tag{9}$$

The derivatives of the boundary conditions (6) in the rotated system are replaced by finite differences. Thus, extrapolation formulae are obtained for calculating the values of the fictitious points:

$$\begin{aligned} U'_{j,k} &= U'_2 - \frac{2\Delta z'}{\Delta x'}(W'_{j,k-1} - W'_{j-1,k}) \\ W'_{j,k} &= W'_2 - \frac{2\Delta z'}{\Delta x'}(1 - 2\beta^2/\alpha^2)(U'_{j,k-1} - U'_{j-1,k}). \end{aligned} \tag{10}$$

All the displacements involved in Equation (10) are at the same time level. Three of the four grid-points involved in the computation are common to the main and the local grid. Only the displacements at point 2 (which is denoted in Fig. 2) are not known. They are approximated by the following linear interpolation:

$$\begin{aligned} U'_2 &= \frac{\varepsilon_1}{\Delta x'} U'_{j,k-2} + \frac{\varepsilon_2}{\Delta x'} U'_{j-1,k-1} \\ \frac{\varepsilon_1}{\Delta x'} &= 1 - 2\sin\theta \\ \frac{\varepsilon_2}{\Delta x'} &= 2\sin^2\theta. \end{aligned} \tag{11}$$

Substituting (9) and (11) in (10) the following equations are obtained:

$$U'_{j,k} = 2\sin^2\theta\, U'_{j-1,k-1} + (1-2\sin^2\theta)\, U'_{j,k-2} - 2\sin\theta\cos\theta\,(W'_{j,k-1} - W'_{j-1,k})$$

$$W'_{j,k} = 2\sin^2\theta\, W'_{j-1,k-1} + (1-2\sin^2\theta)\, W'_{j,k-2} - 2\sin\theta\cos\theta\,(1-2\beta^2/\alpha^2)(U'_{j,k-1} - U'_{j-1,k}). \quad (12)$$

The displacements of the inner points and the horizontal free surface points are computed by Equations (5) and (7) as usual. Then, the values on the fictitious line parallel to the inclined free surface are calculated by formulae (12) in the (x', z') domain and transformed back to the main system, in every time step.

Let us assume that the corner of the wedge is slightly smoothed, and the change of inclination occurs between the two grid points (m, n) and $(m+1, n)$. No special formula is needed for the corner, due to the combination of the composed approximation (7) for the horizontal surface with the extrapolation formulae (12) for the inclined surface. The grid point (m, n) is located on the horizontal surface while $(m+1, n)$ is the first point of the fictitious line. The displacements of the grid points located on the inclined surface are computed by an approximation to the equations of motion (1). A slight modification of formulae (5) had to be made, because they contain displacements of point $(j+1, k+1)$ which is not included in the grid. This grid point is involved in the finite-difference approximation to the cross-derivatives $\frac{\partial^2 U}{\partial x\,\partial z}$, $\frac{\partial^2 W}{\partial x\,\partial z}$ of Equation (1). For the grid points on the inclined free surface the following alternative approximation was used for the cross-derivative:

$$U_{xz} = \frac{1}{4\,\Delta x\,\Delta z}[U_{j+1,k} - U_{j-1,k} - 2\,U_{j-1,k-1} - U_{j,k-1} + U_{j,k+1} - U_{j+1,k-1} - U_{j-1,k+1}] + O(\Delta z). \quad (13)$$

Formulae (12) are suitable for calculating the boundary values on a surface with inclination θ where $1 \geqq \tan(\theta) > \frac{1}{2}$. When $2 > \tan(\theta) \geqq 1$ some modification of the technique is needed. This is discussed in the appendix. The increments are chosen in a manner that $\Delta x = \Delta z/\tan(\theta)$. For a constant Δz, when θ decreases Δx increases, and the number of grid units per pulse width decreases. This may introduce some inaccuracy in the results, as explained by Boore (1972a). In order to avoid this difficulty, the grid for small slopes, $\frac{1}{2} \geqq \tan(\theta) > 0$ is chosen in such a way that $\tan(\theta) = \frac{\Delta z}{l\,\Delta x}$, l is an integer, $l \geqq 2$. In this case the inclined free surface passes through the diagonal of l units, as is illustrated in Figure 12. In this case l rows of fictitious points are needed. On the other hand for steep slopes Δx becomes very small. In this case the time step Δt must be made very small also, in order to satisfy the stability condition (16). Therefore the scheme becomes less efficient. That difficulty can be overcome by appropriate choice of grid units. In that case $\tan(\theta) = \frac{l\,\Delta z}{\Delta x}$, the modification of the main technique for

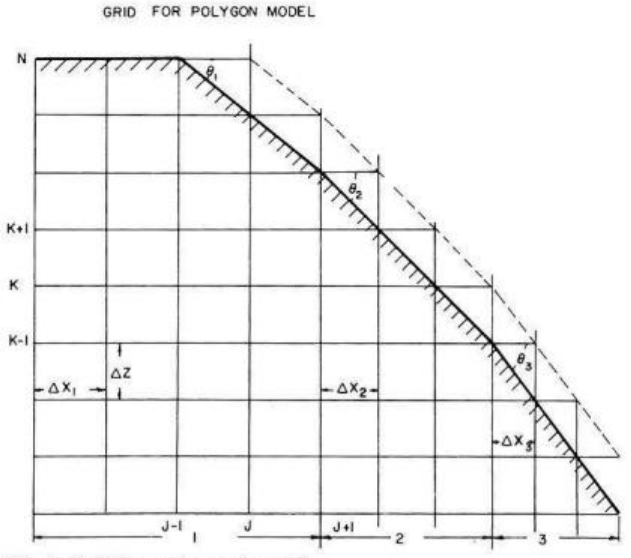

Fig. 3. Grid for polygonal model

the cases of very small or very steep slopes are discussed in the appendix. The next step will be to generalize the method for media with polygonal surfaces.

3. Grid for Polygon Model

Any given topographic profile can be approached by a polygon. Let us construct a rectangular grid with fixed height Δz, and variable width $\Delta x_i \cdot \Delta x_i$ is determined by Equation (4), and is different in every region according to the changing slope θ_i of the surface above. An example for a grid with variable width is shown in Figure 3.

The displacements of every inner point are determined by scheme (5). It contains finite-difference approximations for x derivatives such as:

$$\frac{\partial^2 U}{\partial x^2} = [U(x+\Delta x_i, z, t) - 2U(x, z, t) + U(x-\Delta x_i, z, t)]/\Delta x_i^2. \tag{14}$$

(14) is not completely defined on the boundary between 2 regions with different grid width, because $(x+\Delta x_i, z)$ is not a grid point. In order to enable us to apply formulae (5) on the interface between grids with two different intervals, the displacements at points like $(x+\Delta x_i, z)$ are evaluated by interpolation.

The values on the fictitious lines parallel to the sides of the polygonal surface are computed by extrapolation formulae which represent the boundary conditions. These formulae are obtained with suitable coordinates and local grids, which have been described in the previous section. The computed boundary values are transformed back to the main coordinate system in every time-step.

The technique which has been developed in this paper requires the use of a non-uniform grid, and a non-standard scheme. The unavoidable complexity thus introduced is more than compensated by the ability to simulate the response of real topographic features to seismic waves.

Accuracy and Stability

The polygonal approximation used and the non-uniform grid are liable to cause some problems. The velocity of waves propagating on a grid depends on the grid intervals. Boore (1972a) and Browning et al. (1973) showed that waves propagating on a grid are bound to have a certain phase delay. This delay decreases when the number of grid units per wave length increases. Therefore, any wave which is poorly represented in the coarser grid will change phase speed when passing through an interface into a finer grid. If this wave later passes from the fine grid back into the coarse grid, a serious interaction can result with that part of the wave which has remained in the coarser net. The term "well-represented" wave means: sufficient grid-points per wave length. Browning et al. (1973) also demonstrated that if a wave is already well represented in the coarse net the wave should propagate through the interface between the coarse and the fine grid without difficulty. Taking this consideration into account the parameter of the pulse width was chosen such that

$$6 \max \Delta x_i > \Delta > 5 \max \Delta x_i. \tag{15}$$

This choice (15) is sufficient for proper results. Using larger Δ will cause the pulse to be broad and will result in lack of resolution required for identifying the different body waves.

In order to check the influence of a non-uniform grid on the results the following numerical experiment was made: The displacements due to a P-pulse propagating in a wedge were computed twice, once by a uniform grid, and once by a grid with 2 different Δx such that:

$$\frac{\Delta x_1}{\Delta x_2} = \frac{5}{4}.$$

A comparison between the results is shown in Figure 4. The good agreement between the 2 solutions shows that with careful treatment a non-uniform grid need not cause serious numerical errors. The extrapolation formulae are consistent with boundary conditions, to the first order of accuracy. It is difficult to improve this accuracy, because of the asymmetrical differences to the tangential direction, and the interpolation involved in the computation. For the special case of a 45° slope the differences become symmetric, interpolations are not needed and a second order of accuracy is achieved. If a finite difference scheme is consistent with the differential equations and stable, Lax's equivalence theory states that the numerical results converge to the exact solution as the increments tend to zero (see Richtmyer and Morton, 1967). Alterman and Loewenthal (1970) determined the necessary condition of stability of scheme (5). In order to fulfil this condition locally at any point of the non-uniform grid the following inequality is required:

$$\Delta t \leqq \frac{\text{minimum}(\Delta x_i)}{\sqrt{\alpha^2 + \beta^2 \left(\frac{\text{minimum}(\Delta x_i)}{\Delta z}\right)^2}}. \tag{16}$$

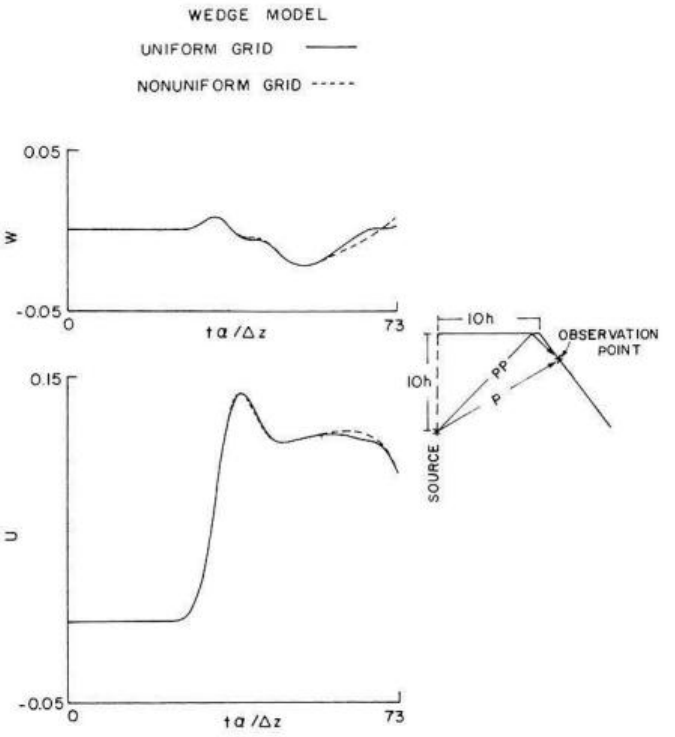

Fig. 4. The displacements as functions of $t\alpha/\Delta z$ on the surface of a wedge, where $\theta = 51.5°$. Comparison between two solutions obtained by: a uniform grid (solid line) and a non-uniform grid (dashed line). The horizontal component below and the vertical one above. $\Delta = 5.5\Delta x_1/\alpha$

(16) applies only to points which are not in the vicinity of the boundaries. This stability condition does not take into consideration the effects caused by introducing the boundary conditions to the scheme. Experimentally it has been found that for the usual relation $\alpha = \sqrt{3}\beta$ the method of incorporating the boundary conditions into the scheme, which has been proposed in this paper, does not disturb the stability.

In order to estimate the error involved when a smooth curve is approximated by a polygon, the problem of a pulse propagating in an elastic cylinder from a line source at its centre was solved. The natural approach is to use cylindrical coordinates and a cylindrical grid. The results are shown by a dashed line in Figure 5. The solid line in Figure 5a shows the displacements on the surface of an octagon circumscribing the cylinder, at the point where the octagon touches the cylinder. There is agreement up to 95% between the solutions until the arrival time of a phase that propagates with Rayleigh wave velocity from the corners along the surface of the octagon. This phase decreases rapidly with depth. When the cylinder is circumscribed by a polygon with 16-sides the amplitude of the diffracted waves decreases by a factor of 2, as can be seen in Figure 5b.

The conclusion of this experiment is that when approximating a smooth curved surface by a polygon, one has to take into account a numerical error

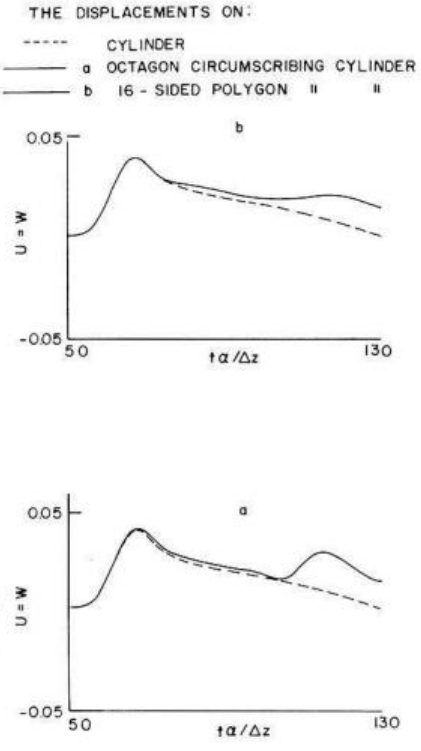

Fig. 5a and b. The displacement as a function of $t\alpha/\Delta z$ on the surface of a cylinder due to a line source at its center (dashed line), in comparison with the displacements on an octagon circumscribing the cylinder (solid line a) and on a 16-sided polygon (solid line b). The radius of the cylinder is $50\Delta z$, and $\Delta = 5.5\Delta z$. The observation point is where the polygon touches the cylinder

which propagates from the corners. This error can be decreased by refining the polygon. When the real topographic profile has such a shape that it contains real corners, these pulses are not errors. They represent the physical phenomenon of diffracted waves.

The Response of Prominent Topographic Features to a Compressional Pulse

The technique that has been developed in the previous sections enables simulation of P-SV wave propagation in prominent features, i.e. features whose deviation from a flat model is larger than or of the same order as the pulse-width. Let us consider two typical topographic profiles, a canyon and a ridge. Figure 6 shows a vertical cross section of a polygonlike canyon. A compressional impulsive source is embedded 10 grid units Δz below the surface, at a horizontal distance of $20\,\Delta z$ from the corner of the canyon. Theoretical seismograms were produced at five sites along the surface of the canyon. Figure 7a, b depicts the horizontal and vertical displacements as functions of the dimensionless time $t\alpha/\Delta z$ at these observation points. The dashed line illustrates the displacements, at the same site of a flat surface. In this case the horizontal displacement is very much amplified and the vertical displacement is slightly attenuated at the upper corner of the canyon. The amplitudes computed on the

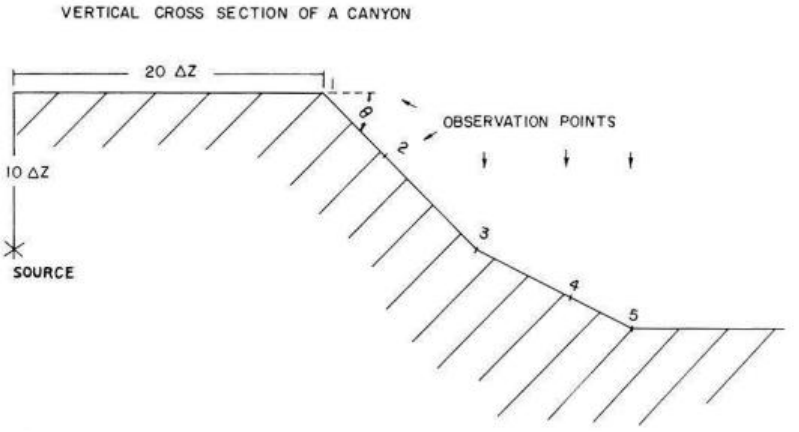

Fig. 6. A vertical cross section of a canyon. θ is 45° at the upper corner, and is made 26.6° at site 3

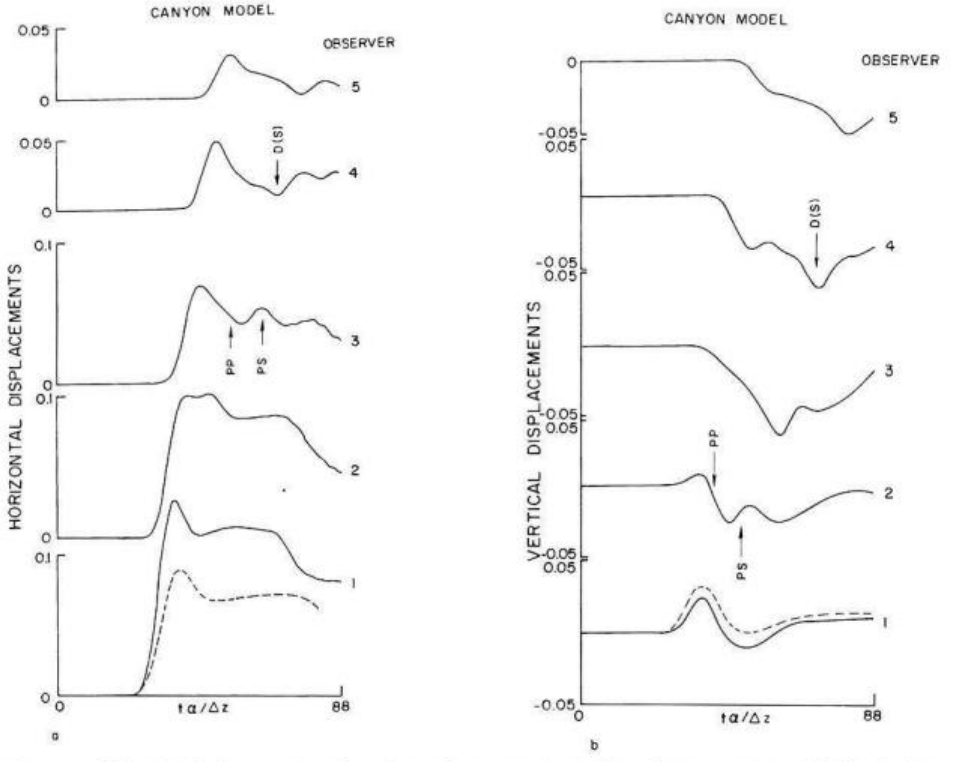

Fig. 7a and b. The displacements as functions of $t\alpha/\Delta z$ on the surface of the canyon model (Fig. 6). The dashed lines are the displacements on a flat model under the same conditions, $\Delta = 5.5\,\Delta z/\alpha$, $D(s)$ denotes the diffracted surface waves

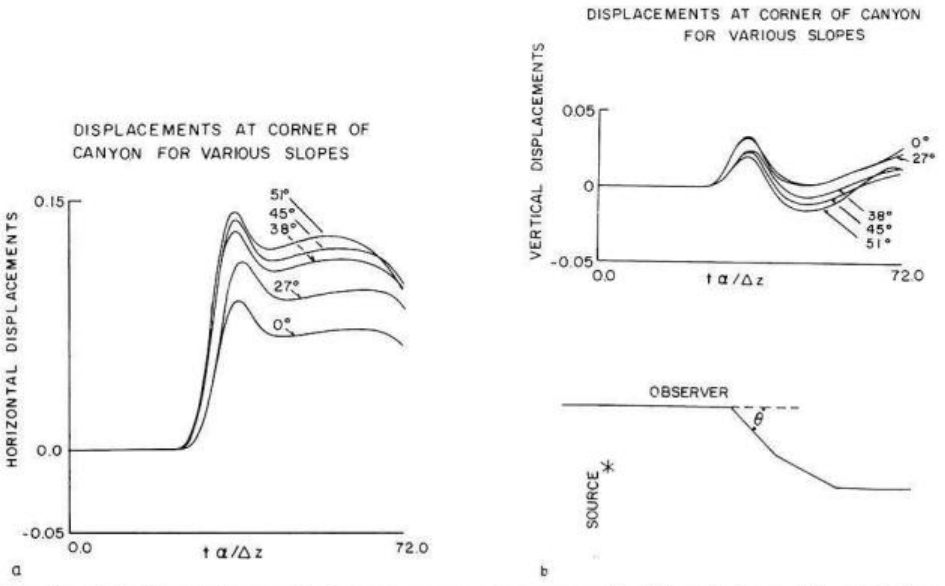

Fig. 8a and b. The displacements at upper corners of canyons with different slopes, $51° \geqq \theta \geqq 0$. The source is at a horizontal distance of $20\Delta z$ from the corner, at depth $10\Delta z$. The horizontal component (**a**) the vertical component (**b**)

flank seem to be unaffected by the topography. The seismograms on the flanks are more complicated. The phases PP and PS reflected from the horizontal surface arrive at sites 2 and 3 after the first pulse. Sites 4 and 5 are in a shadow zone of reflected phases. In these seismograms, the diffracted waves can be clearly distinguished. At the lower corner of the canyon the amplitude is attenuated slightly. An attenuation of 25% was computed at the lower corner of a canyon with vertical borders. This result is in agreement with Bouchon (1973). Trifunac (1973) and Wong and Trifunac (1974) found a considerable amplification of plane SH waves in the upper corner of a cylindrical and an elliptical canyon. For a vertical slope near the corner they found the magnitude of amplification to be greatly dependent on the angle of incidence of the waves. It varied from a few per cent for vertical incidence to nearly 100% for almost grazing waves. Figure 8 shows a comparison between the displacements at upper corners of canyons with different slopes. The surface inclination near the corner varies from 27–51 degrees. The absolute value of the amplitudes increases with the angle of inclination. The magnitude of the computed amplification varies between 20 and 50%. The amplitude of the horizontal displacement depicted in Figure 8a increases considerably when the slope θ increases. The vertical component behaves differently, as can be seen in Figure 8b. Its amplitude decreases slightly when the angle of slope θ increases.

Figure 9 shows a vertical cross section of a ridge model, with a steep slope $\theta = 51°$. The line source is at a depth of $20\,\Delta z$ below the crest.

Figure 10a, b shows the vertical and the horizontal displacements as a function of $t\alpha/\Delta z$ at 5 observation points indicated in Figure 9. The dashed curve is the displacement on the surface of a flat model under the same

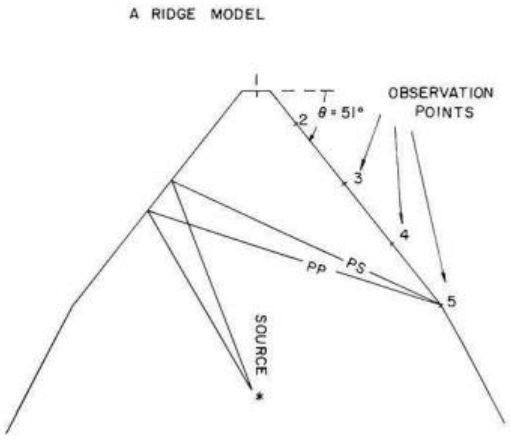

Fig. 9. A vertical cross section of a ridge model

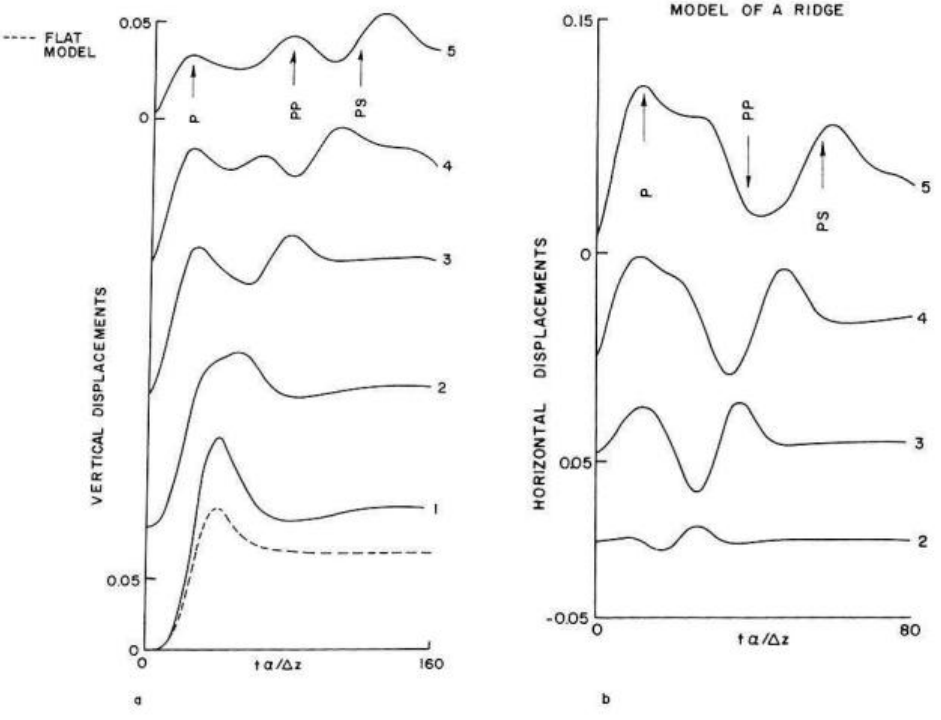

Fig. 10a and b. The displacements as functions of $t\alpha/\Delta z$ on the surface of the ridge model (Fig. 9). The dashed curve is the displacement on a flat model under the same conditions. The horizontal displacements in point 1 are equal to zero

conditions. An obvious amplification is found on the summit. Bouchon (1973) found that the magnitude of amplification depends on the angle of incidence, and varied from 50% for normal incidence to 100% for oblique angles. Bouchon (1973) showed, also, that when the ridge model is made steeper the magnitude of amplification increases. These conclusions are in agreement with our results. When the slope of the ridge model (9) varied between 27 and 51 degrees, the amplitude of the signal increases by 14–52%.

On the flanks Boore (1972b) found amplification of certain frequencies and deamplification of others. He assumed that in the time domain the amplitude of the incident waves would not be changed on the flanks. Bouchon (1973) found attenuation of the incident waves on the ridge flanks. According to our computation the amplitude of P-pulse on the flanks seem not to be affected by topography. Immediately after the first pulse two more pulses were recorded. These were PP and PS waves reflected from the opposite flank. The horizontal component of PP is in the opposite direction to the first pulse. Therefore, for certain sites and relatively long waves the direct and reflected phases may interfere destructively. This may explain why Bouchon (1973) got attenuation on mountain flanks. One can try to explain the high amplitudes on ridge crests as a superposition of the direct and the reflected phases arriving simultaneously at the top. For steep slopes, multireflections also increase the combined amplitude. This focusing effect may even be amplified in a three dimensions model.

Appendix

The computation of boundary values for stress-free surfaces with slopes larger than 45° is slightly different from the technique described in Section (2), but based on the same principle. The difference lies in the fact that a steep surface is closer to the vertical than to the horizontal.

In this case suitable cartesian coordinates are chosen with an angle $\gamma = \pi/2 - \theta$ in the direction counter-clockwise to the main system. In the rotated coordinate system (x^*, z^*) the inclined surface is parallel to the z^* axis. Let (U^*, W^*) denote the displacements in the x^*, z^* directions respectively. The following orthogonal transformation connects the displacements in the two systems:

$$\begin{aligned} U^* &= U\cos\gamma + W\sin\gamma = U\sin\theta + W\cos\theta \\ W^* &= -U\sin\gamma + W\cos\gamma = -U\cos\theta + W\sin\theta. \end{aligned} \tag{17}$$

The boundary conditions required on the inclined stress-free surface are as follows:

$$\begin{aligned} &\frac{\partial U^*}{\partial z^*} + \frac{\partial W^*}{\partial x^*} = 0 \\ &\alpha^2 \frac{\partial U^*}{\partial x^*} + (\alpha^2 - 2\beta^2)\frac{\partial W^*}{\partial z^*} = 0. \end{aligned} \tag{18}$$

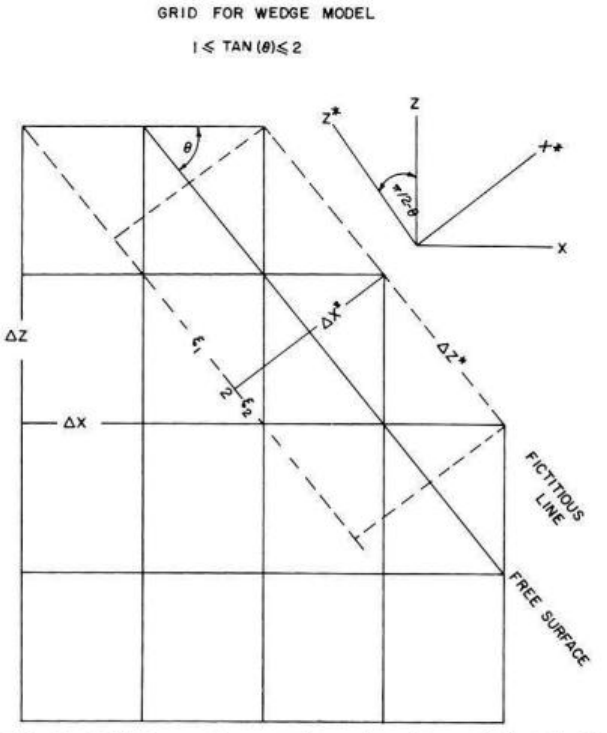

Fig. 11. Grid for a obtuse wedge where $2 > \tan\theta \geqq 1$. (x^*, z^*) are the suitable coordinates, and $(\Delta x^*, \Delta z^*)$ the local grid units

Let us superimpose a local grid around the inclined surface, as shown in Figure 11. The units of this grid are:

$$\Delta x^* = \Delta z \cos\theta$$

$$\Delta z^* = \Delta z / \sin\theta. \tag{19}$$

The derivatives of Equation (18) are replaced by finite differences, and the displacements of point 2 denoted in Figure 11 are evaluated by linear interpolation, such that:

$$\begin{aligned} U^*_{J,k} &= 2\cos^2\theta\, U^*_{J-1,k-1} + (1 - 2\cos^2\theta)\, U^*_{J-2,k} \\ &\quad - 2\cos\theta \sin\theta (1 - 2\beta^2/\alpha^2)(W^*_{J-1,k} - W^*_{J,k-1}) \\ W^*_{J,k} &= 2\cos^2\theta\, W^*_{J-1,k-1} + (1 - 2\cos^2\theta)\, W^*_{J-2,k} \\ &\quad - 2\sin\theta\cos\theta (U^*_{J-1,k} - U^*_{J,k-1}). \end{aligned} \tag{20}$$

Equations (20) are extrapolation formulae to a fictitious grid point at a distance dx^* from the inclined free surface, where $\theta \geqq 45°$. For very small slopes where $\frac{1}{2} > \tan\theta > \theta$ the grid dimensions are chosen in such a manner that the inclined surface passes through the diagonal of 2 or more grid units. As an example, in Figure 12 $\tan\theta = \frac{1}{2}$, in this case a square grid is chosen in such a manner that

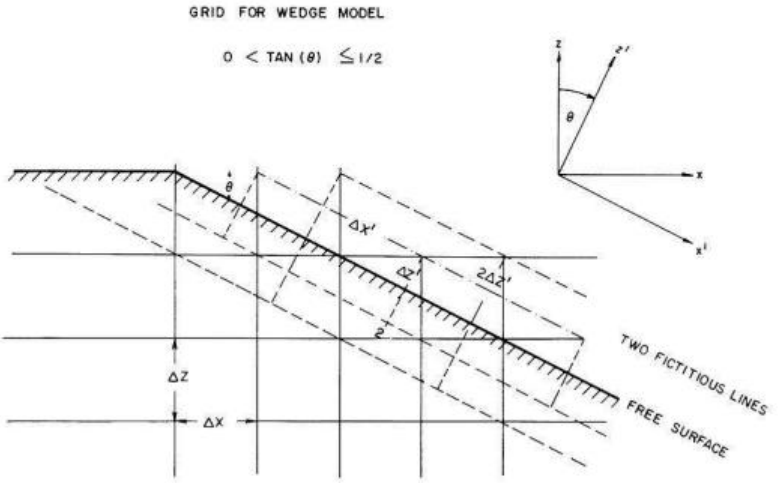

Fig. 12. Grid for an obtuse wedge, where $\frac{1}{2} \geqq \tan\theta > 0$

the surface passes through 2 grid units. Here two fictitious lines are needed. The first at a distance of $\Delta z' = \cos\theta \Delta z$ and the second at a distance $2\Delta z'$ from the surface. ($\Delta z'$ was defined in Eq. (9).) Extrapolation formulae to the first fictitious line are obtained by finite-difference approximations of Equations (6).

$$\begin{aligned} U'_{J,k} &= (1-2\sin^2\theta)\, U'_{J,k-1} + \sin^2\theta (U'_{J-1,k} + U'_{J-1,k-1}) \\ &\quad - \sin\theta\cos\theta (W'_{J+1,k-1} - W'_{J-1,k}) \\ W'_{J,k} &= (1-2\sin^2\theta)\, W'_{J,k-1} + \sin^2\theta (W'_{J-1,k} + W'_{J-1,k-1}) \\ &\quad - \sin\theta\cos\theta (1-2\beta^2/\alpha^2)(U'_{J+1,k-1} - U'_{J-1,k}) \end{aligned} \tag{21}$$

here (J, k) is a grid point on the first fictitious line. Extrapolation formulae for the second fictitious line are obtained similarly.

$$\begin{aligned} U'_{J,k} &= (1-4\sin^2\theta)\, U'_{J,k-2} + 2\sin^2\theta (U'_{J-1,k-2} + U'_{J-1,k-1}) \\ &\quad - 2\sin\theta\cos\theta (W'_{J,k-1} - W'_{J-2,k}) \\ W'_{J,k} &= (1-4\sin^2\theta)\, W'_{J,k-2} + 2\sin^2\theta (W'_{J-1,k-2} + W'_{J-1,k-1}) \\ &\quad - 2\sin\theta\cos\theta (1-2\beta^2/\alpha^2)(U'_{J,k-1} - U'_{J-2,k}). \end{aligned} \tag{22}$$

Acknowledgments. I wish to thank Professor J. Aboudi for suggesting the subject of the present paper. I would also like to express my deepest gratitude to Dr. Dan Loewenthal for helpful advice and important critical comments. This work was supported by the National Resources Research Authority, Ministry of Commerce and Industry, Israel, Grant No. 11329.

References

Aki, K., Larner, K.L.: Surface motion of a layered medium having an irregular interface, due to incident plane SH waves. J. Geophys. Res. **75**, 933–954, 1970

Alterman, Z.S., Loewenthal, D.: Seismic waves in a quarter and three quarter plane. Geophys. J. **20**, 101–126, 1970

Alterman, Z.S., Nathaniel, R.: Seismic waves in a wedge. Bull. Seism. Soc. Am. **65**, 1697–1719, 1975
Boore, D.M.: Finite-difference methods for seismic-wave propagation in heterogeneous materials. In: Methods in Computational Physics, Vol. 11, Chapter 5. New York: Academic Press 1972a
Boore, D.M.: A note on the effect of simple topography on seismic SH waves. Bull. Seism. Soc. Am. **62**, pp. 275–284, 1972b
Boore, D.M.: The effect of simple topography on seismic waves. Implications for the accelerations recorded at Pacoima Dam, San Fernando Valley, California. Bull. Seism. Soc. Am. **63**, 1603–1609, 1973
Bouchon, M.: Effect of topography on surface motion. Bull. Seism. Soc. Am. **63**, 615–632, 1973
Browning, G., Kreiss, H.O., Oliger, J.: Mesh Refinement. Math. Comp. **27**, 29–39, 1973
Davis, L.L., West, L.R.: Observed effects of topography on ground motion. Bull. Seism. Soc. Am. **63**, 283–298, 1973
Ilan, A., Ungar, A., Alterman, Z.: An improved representation of boundary conditions in finite-difference schemes for seismological problems. Geophys. J. **43**, 727–746, 1975
Ilan, A., Loewenthal, D.: Instability of finite-difference schemes due to boundary conditions in elastic media. Geophysical Prospecting **24**, 431–453, 1976
Reimer, R.B., Clough, R.W., Raphael, J.M.: Seismic response of Pacoima Dam in San Fernando Earthquake. Proc. World Conf. Earthquake Eng. 5th, Rome 2, pp. 2328–2337, 1974
Richtmyer, R.D., Morton, K.W.: Difference methods for initial value problems. New York-London-Sydney: Interscience 1967
Trifunac, M.D.: Scattering of plane SH waves by a semicylindrical canyon. Intern. J. Earthquake Eng. Struct. Dyn. **1**, 267–281, 1973
Trifunac, M.D., Hudson, D.E.: Analysis of the Pacoima Dam accelerogram, San Fernando. California, earthquake of 1971. Bull. Seism. Soc. Am. **61**, 1393–1411, 1971
Wong, H.L., Jennings, P.C.: Effects of canyon topography on strong ground motion. Bull. Seism. Soc. Am. **65**, 5, pp. 1239–1257, 1975
Wong, H.L., Trifunac, M.D.: Scattering of plane SH waves by semielliptical canyon. Intern. J. Earthquake Eng. Struct. Dyn. V. **3**, 157–169, 1974

Received November 11, 1976/ Revised Version January 7, 1977